communications engineering

A Nature Portfolio journal

Article

https://doi.org/10.1038/s44172-026-00725-1

Self-deploying reinforced concrete structures

Check for updates

Ezra Ben-Abu [1] ✉, Anna Zigelman[1], Hod Lipson[2] & Amir D. Gat[1]

Formwork for concrete construction remains one of the most resource-intensive, polluting, and constraining components of the construction sector, relying on prefabricated molds that demand extensive material, labor, and on-site preparation. We introduce a self-deploying formwork system based on multistable tubes that transform from a compact configuration to a full-scale structural mold with integrated steel reinforcement. We demonstrate this concept by deploying a steel-reinforced 2.36 m high structure within 14 seconds. We further observed that the polymer shell of the multistable tubes increases the structural strength by a factor of three, significantly enhancing their load-bearing capacity. The demonstrated concept paves the way for the creation of concrete castings with minimal on-site intervention, enabling a scalable pathway toward rapid, low-carbon construction methods.

The reduction of global greenhouse gas (GHG) emissions is one of the most challenging and pressing missions humanity faces today. The construction industry alone accounts for 37% of total GHG emissions[1], with nearly one-third of these emissions coming from the Cross-Laminated Timber (CLT) used in formwork for casting concrete columns, beams, and floors[2–4]. Additionally, up to 75% of building construction time is devoted to formwork[5], and the associated material and labor costs may comprise 35–60% of total building expenses[6]. Therefore, finding alternative construction solutions that do not rely on CLT formwork could significantly reduce global GHG emissions and shorten construction times and costs, making these solutions more environmentally friendly and cost-effective. Concrete construction is typically performed using either cast-in-place methods, which rely on on-site formwork[5,6], or precast methods, where elements are manufactured off-site and assembled on-site[7,8]. While precast construction reduces on-site time, it introduces transportation and lifting constraints, whereas cast-in-place construction remains highly dependent on formwork.

Several formwork methods have been developed as alternatives to CLT formwork, including metal formwork[9–11], which can be also composed of corrugated metallic plates wrapped in helical patterns that enhance shear and axial resistance[12–16], fabric formwork[17–20], CNC-milled styrofoam formwork[21,22], 3D-printed plastic formwork[23–25], mesh mold formwork[26–28], sand formwork[29–31], ice formwork[32–34], and climbing formwork systems designed to improve construction efficiency in repetitive vertical structures[35–37]. The selection of the specific formwork type depends on factors including expected lifespan, geometric complexity, and construction conditions (e.g., weather)[10]. The implementation of such systems in modern architecture often necessitates strategic adaptations, including pre-defined concrete pour points to prevent high-drop casting and mitigate segregation[38–40], or designing formwork to be reused across floors and even between buildings[41–44]. These strategies help streamline on-site preparation and reduce the amount of cross-laminated timber (CLT) required in each project. However, conventional formwork systems face significant limitations, as they are inherently time consuming for standard geometries, and become particularly inefficient when applied to complex configurations. In such cases, they require highly customized designs that are difficult to implement, further increasing construction time and cost.

More recently, construction techniques that do not rely on any formwork have emerged. One of the most recognized methods is the 3D printing of small houses[45–49], for which reinforcement solutions have also been proposed[50–54]. Another approach involves the use of pneumatic actuation to inflate the entire reinforced concrete shell of a structure, followed by concrete spraying after inflation[55–58]. Additional methods have been developed for creating complex structures without concrete, using deployable systems that can be inflated with fluids[59–61], deployed manually[62–64], or supported by polyurethane foam[65–67], which solidifies upon drying and provides structural stability. These structures are typically based on inflatable structures such as origami-based structures[68–73] or thin-walled corrugated tubes[74–77]. In spite of the aforementioned advances, the existing approaches rely on external actuation, lack integration between formwork and structural function, or are limited in scalability and structural performance, making it imperative for a method that can deploy rapidly and maintain structural integrity while maintaining geometric flexibility.

In this study, we present a self-deploying formwork concept for reinforced concrete structures. Specifically, we investigate whether shape-morphing interconnected multistable tubes can (i) rapidly deploy into predefined structural configurations, (ii) maintain sufficient structural performance after concrete casting and curing, and (iii) provide practical

[1]Department of Mechanical Engineering, Technion—Israel Institute of Technology, Haifa, Israel. [2]Department of Mechanical Engineering, Columbia University, New York, NY, USA. ✉e-mail: ezrab@campus.technion.ac.il

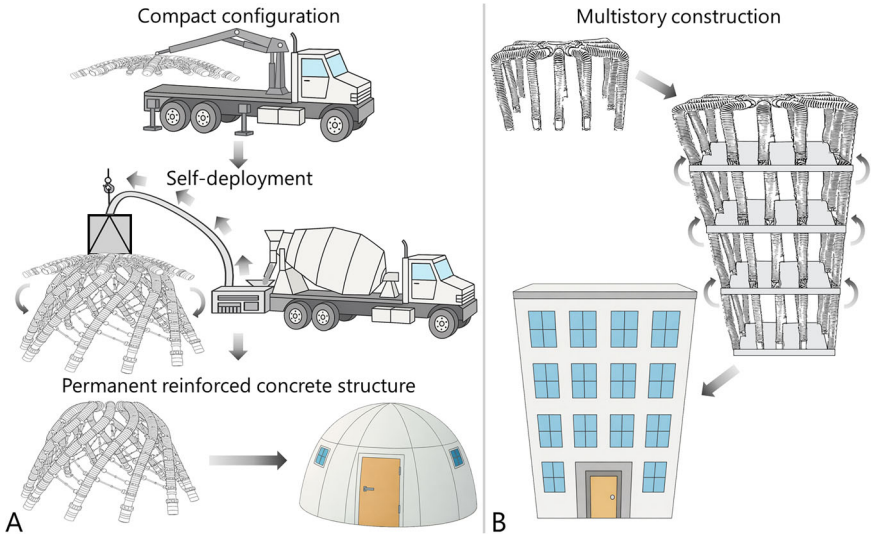


Fig. 1 | An illustration of the proposed concept. **A** A three-stage process for constructing a permanent reinforced concrete structure. First, the closed and compact structure, which was assembled in a factory, is delivered and installed at the desired location. Second, the structure is rapidly deployed by direct pumping of the concrete. In this procedure, concrete is poured by a concrete truck into a concrete pump, which then pours it into the structure that is automatically self-deployed due to gravity. Finally, after the structure is fully deployed and hardened, the temporary stand is removed, and the obtained skeleton is covered with isolated panels, windows, and a door. **B** Similar procedure can be employed also for constructing a multistory building, each floor constructed according to (**A**), to achieve the skeleton of the building. At the last stage the building may be covered as needed.

advantages over conventional formwork approaches in terms of construction efficiency and sustainability. This method relies on shape-morphing interconnected multistable tubes, guided either by director field theory[60] to achieve complex geometries, or by a constrained ceiling, where columns expand due to gravity to form more conventional 3D shapes. We experimentally demonstrate the deployment of such structures in the meter scale in less than a minute. Such rapid deployment does not only accelerate the construction process, but also minimizes concrete segregation, which simplifies the casting procedure. To ensure structural integrity, we incorporate flexible steel cables to accommodate elastic deformation during deployment and use helical tube designs, that improve shear and axial resistance. We also derive a theoretical model for the final configuration based on the amount of concrete and the initial conditions. In addition, experimental measurements showed that the polymer shell surrounding the multistable tubes increases the structural strength of the final reinforced concrete element by a factor of three, substantially enhancing its load-bearing capacity without adding significant weight.

Results

As illustrated in Fig. 1, our approach consists of the following stages. First, a compact, closed structure is assembled in a factory with integrated steel reinforcement, according to a predefined requirements, which refer to the desired final geometry of the structure. Specifically, based on the target geometry, the arrangement of the multistable tubes and the placement of the connectors are determined to ensure that the structure deploys into the intended configuration. The steel cables are incorporated as part of the reinforcement system, providing the necessary tensile strength for the cured concrete. The structure is then delivered and installed at the construction location. Next, concrete is poured by a concrete pump, which then pours it into the structure that is automatically self-deployed due to gravity. Note that although in the present study, we used a water-cement mixture, the proposed method is fully compatible with self-compacting concrete. Finally, after the structure is fully deployed and cured the obtained skeleton is covered with isolated panels, windows, etc. See Fig. 1A.

Harnessing multistability for deployable formwork design

In this section, we show our experimental results for rapid formwork deployment of various geometries and sizes, where in all cases the multistable tubes are reinforced by two steel cables. Note that, in centimeter-scale cases, we use an external pressure to achieve the deployment, since at smaller scales, gravity is not sufficiently dominant. However, in the meter-scale experiment, the gravity is very dominant and the structure has the ability to self-deploy without the need for any external forces.

In Fig. 2, we show an illustration of the deployment process for a multistory building composed of two rectangular box-shaped floors, a cone shape, and a sphere shape. In all three cases, we first present the top view of the initial compact configuration (see panels (A1), (B1), and (C1)). Then, we show the isometric view of the initial (marked by transparent blue) and final shape of all configurations (see panels (A2), (B2), and (C2)), thus visualizing the deployment process (for the deployment dynamics, see Movie S1). Note that the connectors between the straws in panels (B) and (C) were placed according to the model in ref. 60. Note that the primary role of the connectors in our system is geometric, rather than structural. The connectors guide and constrain the multistable tubes during deployment, ensuring that the structure reaches the desired final geometry and maintains the prescribed spatial arrangement between neighboring elements. Importantly, the connectors are not intended to contribute to the mechanical strength of the final structure. After the concrete is cast and cured, the load-bearing capacity is governed by the reinforced concrete itself, and the connectors can be removed without affecting the structural performance. In panel (A3), we show an illustration of the attachment of two floors in order to construct a multistory building. Moreover, an example of the height-adjustment property is illustrated by the black stair in panels (B3) and (C3), which highlight the self-leveling nature of the structure at various terrains.

In Fig. 3, we demonstrate the resistance and strength of the proposed structures. In particular, Fig. 3A illustrates the load stability of the centimeter-scale spherical structure by showing in (A1) its ability to support a 95 kg man standing and jumping on top of it. In panels (A2)-(A4), we demonstrate the jumping test, where the maximum jumping height in (A3) was 15 cm (for the jumping test, see Movie S1). Figure 3B presents the experimental setup for both compression and buckling tests under axial loading. The graphs in Fig. 3C1–C3 show the applied axial load versus the displacement of the tested columns in various cases, including buckling and compression for helical folding tubes (HFTs) and conical frusta tubes (CFTs) (*sheathed* and *bare*), each measurement repeated 3 times. The options "sheathed" and "bare" refer to the tested columns in which the thin plastic shell was left as is and removed after concrete solidification, respectively. To minimize imperfections in the tested columns and to ensure loading conditions that approximate pure compression and buckling, we selected slenderness ratios of $l/d = 1$ and $l/d = 12$, respectively, where l denotes the column length and d is the outer diameter of the tested columns. All measurements were performed four weeks after the concrete casting. The tests were conducted under displacement-controlled conditions, with a loading rate of 3 mm/min. For the bare specimens, the tests were continued until failure. For the sheathed specimens, the tests were terminated upon reaching a plateau in the load-deformation response. At this stage, the internal concrete was already significantly crushed and confined by the

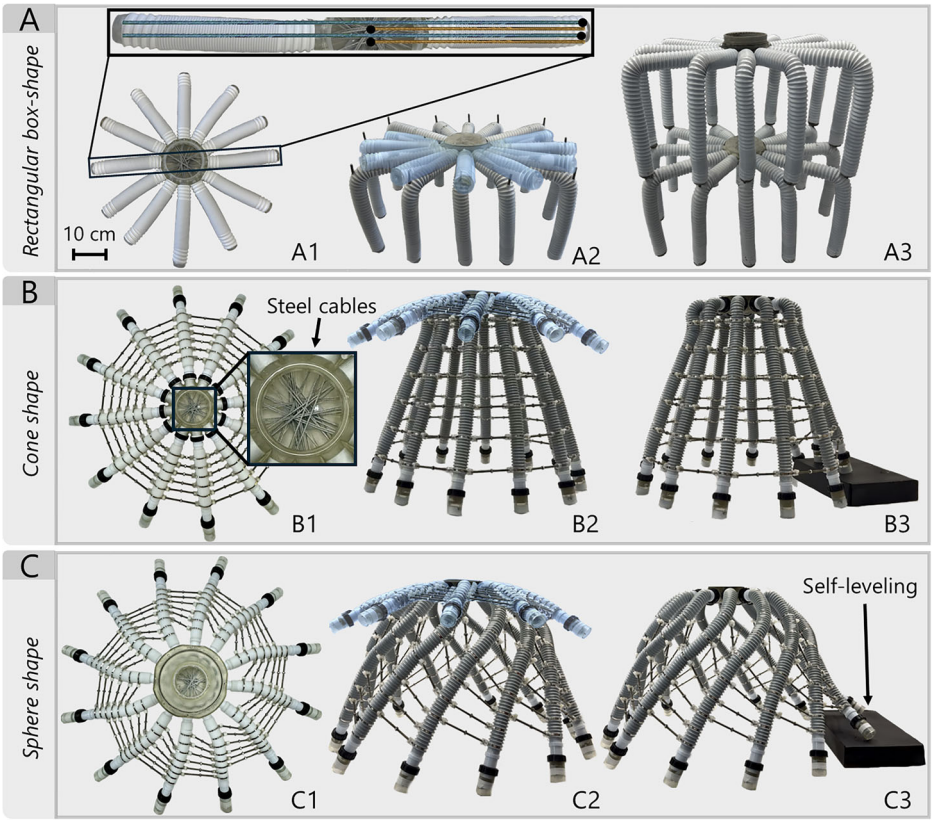


Fig. 2 | A demonstration of centimeter-scale reinforced concrete structures. A An illustration of the deployment process for a multistory building composed of two rectangular box-shaped floors. **A1** Top view of the initial compact configuration with an inset that illustrates the steel cables position within the tubes, where the black dots represent fixed ends. **A2** Isometric view of the initial (marked by transparent blue) and final configurations of a rectangular box-shaped floor. **A3** An illustration of the attachment of the second floor to the first one (both deployed as shown in (**A2**)), visualizing the concept of the modularity. **B**–**C** An illustration of the deployment process for a cone and a sphere shape, respectively. **B1, C1** Top view of the initial compact configuration, where connectors between the straws were placed according to the model in ref. 60. **B2**, **C2** Isometric view of the initial (marked by transparent blue) and final configurations of a cone and a sphere shape, respectively. **B3**, **C3** Demonstration of the self-leveling nature of the structure, where the black stair indicates the ability to adjust the height during deployment. The inset in (**B1**) is an increased view of the center part of (**B1**), which visualizes the steel cables placement. The scale bar corresponds to 10 cm.

polymer shell, such that the measured response no longer reflected the true load-bearing capacity of the structural element. The solid curves in Fig. 3C1–C3 represent the mean result over 3 experiments and the shaded areas correspond to the regions between minimum and maximum of these measurements. It is possible to see that the sheathed samples are approximately three times stronger than the bare samples and that the HFT samples are approximately twice as strong as the CFT samples, suggesting that sheathed HFTs provide the best performance for reinforced concrete columns. The observed increase in load-bearing capacity of sheathed samples can be qualitatively attributed to a confinement effect. In the unconfined case, the concrete fails once a critical displacement is reached, associated with crack initiation and localized deformation. When enclosed by the polymer shell, lateral deformation is constrained, limiting the displacement modes that lead to failure. This confinement delays crack development and failure, allowing the structure to sustain higher loads. Thus, the polymer shell does not increase the intrinsic material strength, but rather delays the failure mechanism, resulting in an enhanced load-bearing capacity. Moreover, note that in all cases the results indicate that the columns meet the strength requirements of the ASTM C39 standard.

In Fig. 4(A1), (A2), and (A3), we show a sequence of frames from a video (see Movie S1) of the self-deployment of the meter-scale structure at times $t = 0$, 6, and 14 seconds, respectively. In Fig. 4B, we show a sequence of frames from a simulation showing a good agreement between the experiment and the numerical simulation of the deployment, which was performed according to the model described in SI. Our model is designed to allow a prediction of the final shape of the deployed structure and its stability as a function of the initial configuration and various physical parameters, such as the multi-stable tubes' stiffness, the concrete flow-rate, etc. Note, however, that the rheological behavior of fresh concrete, including its viscous and non-Newtonian characteristics, is not incorporated into the modeling framework. This limitation will be addressed in future work. In Fig. 4C, we show the final result of the meter-scale experiment (shown in panel (A)), where the dimensions of the final structure are 2.4 m base diameter and 2.36 m height. Moreover, the structure adapts to uneven terrain with a height variation of 13 cm, without the need for external adjustment. In order to visualize the dimensions of the cone shape structure, two people are standing inside of it. Note that after the concrete had cured, all eight tubes were anchored with four steel rods per tube (40 cm deep) and cast with small individual concrete footings.

Discussion

First, let us compare the proposed deployment method with the construction methods mentioned in the Introduction. Specifically, the proposed method differs from the existing approaches such as 3D printed construction, pneumatic membrane based systems, and advanced formwork techniques used in the construction sector. While these methods rely on external processes such as layer-by-layer deposition, air pressure, or rigid molds to define the geometry, the present approach achieves shape morphing through the deployment of a multistable structure during casting. This enables rapid transformation from a compact configuration to the final geometry while maintaining control over the structure throughout the process. Moreover, in the current study, the structure is deployed onto a temporary support system that can be easily removed after curing. In future work, the system can be designed such that the multistability of the tubes, together with the connection design, provides sufficient stability to maintain the structural configuration throughout the curing process. This would eliminate the need for external support by a suspension system such as a temporary stand or a crane after the deployment is complete.

Note that several additional aspects will be investigated in future work, as discussed below. A more detailed analysis of the achievable tolerances, as well as the design of connections and joints will be performed. These studies will define the acceptable ranges that must be maintained and will ultimately determine the required tolerances for a manufacturing process. Once these tolerances and design constraints are established, it will be necessary to ensure that the activation threshold of the multistable tubes remains significantly lower than the forces applied by the concrete during casting. This will ensure reliable deployment of the structure, even in the presence of variability between different tubes. Moreover, in order to meet the fire safety

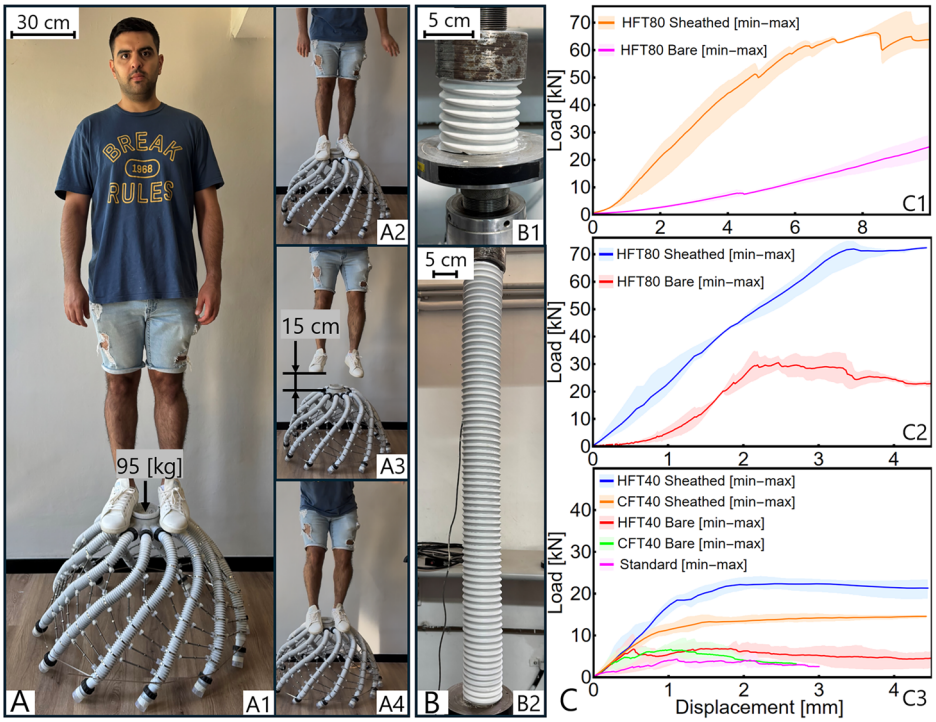


Fig. 3 | Compressive strength tests of concrete columns under axial loading. A Demonstration of the load stability of the proposed structures. **A1** A spherical shape structure made of 40 mm diameter sheathed CFTs supports a 95 kg man standing and jumping on top of it. **A2**–**A4** Three frames of the jumping test, where the maximum jumping height in (**A3**) was 15 cm. **B** Illustration of experimental setup for axial loading measurements for compression and buckling in (**B1**) and (**B2**), respectively. **C** Experimental measurements of axial load (in kN) versus column displacement (in mm), where the solid curves represent the mean result over 3 experiments and the shaded areas, which correspond to the regions between minimum and maximum of these measurements are denoted by [min-max]. For (**C1**) and (**C2**), we used sheathed and bare 80 mm diameter HFTs under buckling and compression, respectively. For (**C3**), we employed sheathed and bare 40 mm diameter HFTs and CFTs, as well as a standard circular 40 mm diameter column under compression. The scale bars in (**A**) and (**B**) correspond to 30 cm, 15 cm, and 5 cm.

requirement, in future implementations, we will replace the flammable polymer tubes with metallic multistable tubes, which could also serve as an additional structural reinforcement component. Furthermore, this replacement to metallic multistable tubes will allow to maintain load-bearing capacity for larger diameters.

Next, let us discuss the expected environmental and economic advantages of the proposed system. As cited in the Introduction, conventional formwork typically accounts for approximately 35–60% of total construction cost and up to 75% of construction time, while also contributing significantly to material waste and carbon emissions due to the extensive use of temporary molds. Contrary, the proposed system eliminates the need for external formwork by integrating the formwork function into the deployable structure itself. This leads to several key advantages: a substantial reduction in material (mainly CLT molds) usage, a significant decrease in labor and assembly time due to rapid deployment (seconds to minutes instead of hours to days), and reduced environmental impact associated with formwork production, transportation, decreasing the need for trees harvesting, and disposal.

The reported cost and CO_2 emission values in Table 1 represent first-order estimates based solely on material consumption and production. Costs associated with transportation, installation, labor, maintenance, reuse, and end-of-life processing were not considered. Based on material costs alone, the proposed PP-based formwork used for concrete is estimated to cost approximately 11 USD/m^3, compared with approximately 193 USD/m^3 for conventional CLT formwork used for concrete. Furthermore, conventional formwork systems typically require additional supplies and substantial on-site labor for assembly, installation, and removal. In the reference study of conventional formwork used for concrete[6], the total formwork cost, including supplies and labor, reached approximately 1710 USD/m^3. By contrast, the proposed self-deploying formwork requires minimal on-site formwork operations, suggesting additional potential cost savings beyond the material costs considered here. For the construction-time estimate, the conventional formwork value was normalized from a reported 43.3 h formwork-installation task performed by four workers for 13.6 m^3 of concrete[6], corresponding to approximately 12.7 labor-h/m^3 for concrete. The corresponding value of the proposed PP method was obtained from the deployment of a 0.113 m^3 structure in 14 s.

Finally, let us discuss possible failure scenarios during the deployment process. Specifically, asymmetric filling may lead to uneven deployment of different tubes. This failure can be mitigated by maintaining a controlled and continuous inflow, which promotes a stable propagation of the filling front. The geometric constraints of the structure further help to guide the deployment properly. Local blockage failure may lead to air pocket regions which can affect the overall structural strength. The occurrence of this failure may be significantly reduced by using sufficiently large tube diameters and appropriate concrete mixtures with high workability. The current deployment model does not explicitly account for the rheological behavior of fresh concrete, including viscosity and yield-stress effects. Nevertheless, the deployment process occurs on a timescale of seconds, whereas concrete setting and significant rheological evolution typically occur over substantially longer timescales. A premature setting of the concrete failure is not expected to occur at all. This is because the deployment process timescale is much shorter than the typical setting time of the concrete. In our meter-scale experiments, the structure fully deploys within seconds, while concrete setting occurs over much longer timescales. Therefore, the system reaches its final configuration well before any significant stiffening takes place.

Conclusions

In this study, we demonstrated that shape-morphing interconnected multistable tubes can serve as self-deploying formwork for reinforced concrete structures. We showed that such structures can rapidly deploy into predefined configurations, maintain structural performance after casting and curing, and provide practical advantages over conventional formwork approaches. We further demonstrated the feasibility of deploying both traditional structural configurations, such as rectangular box-shaped structures, and more complex nontraditional geometries, including conical and spherical configurations. The proposed design enables rapid deployment of reinforced concrete structures through a single inlet, while its self-leveling nature enhances robustness and adaptability to various terrains.

Here, we presented experimental demonstration for the deployment of up to meter-scale structures of various shapes, where all experiments lasted less than a minute.

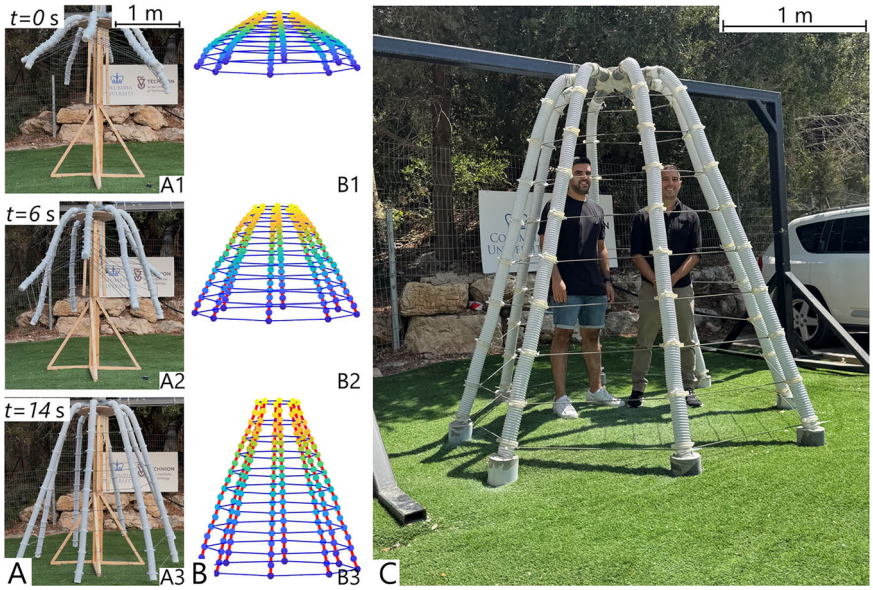


Fig. 4 | Meter-scale experiment. A A sequence of frames from a video (see Movie S1) of the self-deployment of the meter-scale structure at times $t = 0$, 6, and 14 seconds. **B** A sequence of frames from a simulation showing a good agreement of the deployment between the experiment and the model. **C** A demonstration of the final configuration (resulting from the experiment shown in (**A**)) of the meter-scale self-deployed reinforced concrete cone shape with a man standing inside of it, serving as a reference to the deployed structure. The scale bars correspond to 1 m.

Table 1 | A comparison between conventional formwork systems and the proposed self-deploying formwork concept

Metric	Conventional formwork	Proposed method
Environmental impact	Estimated material-production emissions are ~ 32 kg CO_2e/m^3 for concrete in a 17 mm thick CLT mold[78].	Estimated material-production emissions are ~ 14 kg CO_2e/m^3 for concrete in a 0.2 mm thick PP tube[79].
Material cost	Estimated material cost is ~ 193 USD/m^3 for concrete in conventional CLT formwork[6].	Estimated material cost is ~ 11 USD/m^3 for concrete in the proposed PP formwork[80].
Construction time	Formwork installation for concrete is ~ 3.2 h/m^3[36].	Self-deployment for concrete is ~ 0.034 h/m^3.
Concrete casting	Multiple pour points may be required[38–40]	Single-inlet casting demonstrated

Furthermore, our self-deploying formwork method minimizes segregation effects due to the expansion of the multistable tubes during deployment, thus simplifying the design of the concrete pouring procedure relative to the traditional formwork methods. Moreover, in order to ensure structural strength, we employed the following two strategies. First, we installed flexible steel cables, which allow complex elastic distortions during the deployment of the structure, thus providing additional reinforcement beyond the outer reinforcement of the multistable tubes. Second, we used helical multistable tubes, which, according to refs. 14–16, provide a better shear and axial resistance of the reinforced concrete columns. Furthermore, we discovered that a thin plastic shell of the multistable tubes increases the structural strength of the structure by a factor of three, substantially enhancing its load-bearing capacity without adding significant weight. In addition, we proposed a theoretical model and compared the simulation and experimental results, which yielded a good agreement. Thus, our concept is accompanied by a validated theoretical tool, which should be capable of predicting stability and final configuration as a function of the initial setup.

The structures demonstrated here are still relatively small compared to typical buildings. Additional research will be needed to establish the viability of this approach to structures tens of meters height. Similarly, additional research is needed to understand the durability of the proposed method under dynamic loading, as well as alternative sheathing and reinforcement materials. Note that since the concrete that will be used in real building systems is the same as used in standard construction techniques, our methodology is expected to sustain at least the same load-bearing capacity as the traditional buildings. The present study does not address the response of meter-scale constructions under lateral loads, and investigating such behavior remains an important direction for future work. The applicability of the proposed methodology to multi-story buildings has not been established in the present study and remains conceptual at this stage. Future work should investigate the effects of structural height on stiffness characteristics, potential buckling limits, and overall structural stability in multi-story configurations. An additional limitation of the current implementation is the use of single-use polymer tubes, whose environmental impact has not yet been fully assessed. A comprehensive life cycle assessment will be required in future work to evaluate the overall sustainability of the proposed approach and to explore alternative materials or reusable configurations. Moreover, future work will address inter-floor connections, reinforcement continuity, and overall structural stability. Similarly, constraints related to architectural features, such as windows and doors, will be addressed through careful design of the structural layout.

Beyond technical advances, our work has the potential to redefine the construction methodology of reinforced concrete structures, particularly in situations requiring rapid and scalable assembly, such as large-scale infrastructure projects. Overall, our approach offers a more adaptable, sustainable, and cost-effective model for future architecture compared to 3D printed construction, pneumatic membrane based systems, and advanced formwork techniques used in the construction sector.

Methods

In this study, we propose a self-deploying formwork method for the rapid deployment of reinforced concrete structures. Our approach is based on a structure, which consists of multiple multistable tubes. One end of all tubes is attached to a 3D-printed circular part, so that the whole configuration is axisymmetric. The other end of the tubes is partially sealed by a 3D-printed component, so it allows excess water to drain from the system. Inside all of the multistable tubes there are two (overlapping) regions with two steel cables in each region, so that when the tube deploys there exist at least two cables along its length. The diameter of these cables is equal to 10% of the tube's radius. This configuration ensures reinforcement along the entire

length of the tube in the deployed state. Each steel cable consists of flexible multi-strand steel cables (twisted wire ropes), made of several thin steel wires helically wound together. The cables were used without any special surface treatment. Note that the interaction between the cementitious material and the steel cables is mainly based on friction and mechanical interlocking due to the multi-strand geometry of the cables.

Modeling details

Our approach is based on the assumption that a bandy straw can be modeled as a sequence of nodes which are connected by elastic springs. Each node in this chain is responsible for holding the mass of the fluid (or concrete) within the straw in its vicinity, where masses m_i of all nodes along the straw sum up to the mass of the straw. Each node whose location is $\mathbf{x}_i = (x_i, y_i, z_i)$ moves according to the Newton's second law, $d^2\mathbf{x}_i/dt^2 = \mathbf{F}^i_{\text{tot}}/m_i$, where the total force $\mathbf{F}^i_{\text{tot}}$ accounts for gravity and elastic forces of the springs connected to the node. The springs connecting the nodes along the straw are assumed to be elastic, with stiffness k_r. Similarly to the experiment, the straws are assumed to be connected with the connectors (whose masses are negligible relative to the masses of the straws), which are also modeled as elastic springs with stiffness k_b, so that $k_b \gg k_r$. Note that although we assume that all joints between the straws and the connectors always contain nodes, to increase the accuracy of the model, there might exist nodes along the straws also between the joints, but not only on the joints themselves. For more details, see SI.

Fabrication and experimental setups

All 3D-printed components were fabricated using SLA 3D printer (Form 3BL). The zip ties and connectors were made of stainless steel. The concrete used in all experiments consisted of a 50:50 mixture of water and standard Portland cement. The fluid reservoir was constructed from two 3D-printed parts and a Perspex tube with inner and outer diameters of 190 mm and 200 mm, respectively. The connectors were made from M6 threaded rods.

Centimeter-scale experiments were constructed using 40 mm polypropylene either conical or helical multistable tubes connected to the fluid reservoir, which was connected to a pressure controller (ELVEFLOW OB1 MK3+) and, in turn, to a compressor (CompAir L07).

The meter-scale experiment was constructed using 80 mm polypropylene helical multistable tubes connected to the fluid reservoir, which was connected to a pump (Afec LBV 40A 400W 7m) submerged in a 240 L container. The closed structure was placed on a stand with a height of 2.36 m and a base of 2.4 m, made from pine wood rods. Note that the multistable tubes with various diameters up to 16 cm are commercially available. However, there are no technical limitations for producing such tubes at larger diameters, according to demand.

The axial loading experiment was conducted using MTS machine retrofitted with Instron 250 kN system. Each type of column was tested three times and all measurements were performed 28 days after the concrete casting. The samples consisted of sheathed and bare HFTs and CFTs with outer diameters of 40 mm and 80 mm, as well as a standard bare circular column.

The photos in Figs. 2 and 3, and the frames of the experimental setup shown in Figs. 2 and 4 were extracted from videos, all of which were captured using iPhone 15 Pro Max camera in 4K resolution at 60 fps.

Data availability

Source data underlying the figures presented in this study are publicly available via Figshare at: https://doi.org/10.6084/m9.figshare.32597784.

Code availability

The deployment simulations were implemented using a custom MATLAB script based on the model described in the SI. The code is available via Figshare at: https://doi.org/10.6084/m9.figshare.32597784.

Received: 15 March 2026; Accepted: 25 June 2026;
Published online: 23 July 2026

References

1. United Nations Environment Programme. Building materials and climate: Constructing a new future https://www.unep.org/resources/report/building-materials-and-climate-constructing-new-future (2023).
2. Nakano, K., Karube, M. & Hattori, N. Environmental impacts of building construction using cross-laminated timber panel construction method: a case of the research building in Kyushu, Japan. *Sustainability* **12**, 2220 (2020).
3. Gappmaier, P., Reichenbach, S. & Kromoser, B. Advances in formwork automation, structure and materials in concrete construction. *Autom. Constr.* **162**, 105373 (2024).
4. Makoond, N., Setiawan, A., Buitrago, M. & Adam, J. M. Arresting failure propagation in buildings through collapse isolation. *Nature* **629**, 592–596 (2024).
5. Terzioglu, T., Polat, G. & Turkoglu, H. Analysis of formwork system selection criteria for building construction projects: a comparative study. *Buildings* **11**, 618 (2021).
6. Kreiger, E. L., Kreiger, M. A. & Case, M. P. Development of the construction processes for reinforced additively constructed concrete. *Addit. Manuf.* **28**, 39–49 (2019).
7. Gerwick Jr, B. C. *Construction of Prestressed Concrete Structures* (John Wiley & Sons, 1997).
8. Levitt, R. E. & Samelson, N. M. *Construction Safety Management* (John Wiley & Sons, 1993).
9. Gao, K., Xu, J., Zhu, Y., Zhang, Z. & Zeng, Q. Study on the technology and mechanism of cleaning architectural aluminum formwork for concrete pouring by high energy and high repetition frequency pulsed laser. In *Photonics*, vol. 10, 242 (MDPI, 2023).
10. Coniglio, N., Spitz, N. & El Mansori, M. Designing metallic surfaces in contact with hardening fresh concrete: a review. *Constr. Build. Mater.* **255**, 119384 (2020).
11. Abreu, M. M. D. & Lordsleem Jr, A. C. Aluminum formwork system: loss and productivity. *Built Environ. Proj. Asset Manag.* **9**, 616–627 (2019).
12. Fang, Y., Liu, C., Yang, H. & Yang, L. Axial behaviour of concrete-filled corrugated steel tubular column embedded with structural steel. *J. Constr. Steel Res.* **170**, 106064 (2020).
13. Sun, H., Zhang, L., Liu, Y., Liu, B. & Feng, M. Axial compression behavior of large-diameter, concrete-filled, thin-walled galvanized helical corrugated steel tubes column embedded with rebar. *Buildings* **14**, 24 (2023).
14. Fang, Y., Wang, Y., Yang, H. & Lin, X. Experimental behavior of concrete-filled thin-walled corrugated steel tubes with large helical angles under monotonic and cyclic axial compression. *Thin-Walled Struct.* **173**, 109043 (2022).
15. Fang, Y., Yang, H., Chan, T. & Wang, Y. Experimental investigation on seismic behaviour of concrete-filled corrugated steel tubes under cyclic torsional loads. *Eng. Struct.* **309**, 118062 (2024).
16. Wang, G., Wei, Y., Zhang, Y., Liu, L. & Lin, Y. Experimental behavior of concrete-filled double-skin tubular columns with outer galvanized corrugated steel tubes under axial compression. *Eng. Struct.* **295**, 116856 (2023).
17. Orr, J. J., Darby, A. P., Ibell, T. J., Evernden, M. & Otlet, M. Concrete structures using fabric formwork. *Struct. Eng.* **89**, 20–26 (2011).
18. Veenendaal, D., West, M. & Block, P. History and overview of fabric formwork: using fabrics for concrete casting. *Struct. Concr.* **12**, 164–177 (2011).
19. Tahmoorian, F., Nemati, S. & Soleimani, A. A state of the art on the structural performance of fabric formwork systems. *Eng. Solid Mech.* **8**, 49–62 (2020).
20. Cauberg, N., Parmentier, B., Vanneste, M. & Mollaert, M. Fabric formwork for flexible, architectural concrete. In *Proceedings of the International Symposium on Fibre-Reinforced Polymer*

Reinforcement For Concrete Structures, FRPRCS-9. Sydney, Australia (2009).
21. Mainka, J., Kloft, H. & Stein, E. A novel precise formwork-technology based on CNC milled recyclable industrial wax for the casting of geometrically complex concrete elements. In *Proceedings of IASS Annual Symposia*, vol. 2015, 1–12 (International Association for Shell and Spatial Structures (IASS), 2015).
22. Susic, I. & Baseta, E. Foam and solvent: a low-tech self-forming casting technique for the production of double-curved asymmetrical concrete panels. In *Proceedings of the IASS 2024 Symposium: Redefining the Art of Structural Design, Zurich, Switzerland, August 26–30, 2024*. (International Association for Shell and Spatial Structures (IASS), 2024).
23. Jipa, A. & Dillenburger, B. 3d printed formwork for concrete: State-of-the-art, opportunities, challenges, and applications. *3D Print. Addit. Manuf.* **9**, 84–107 (2022).
24. Jipa, A., Bernhard, M. & Dillenburger, B. Submillimeter formwork: 3d-printed plastic formwork for concrete elements. In *2017 TxA Emerging Design+ Technology Conference Proceedings*, 70–79 (Texas Society of Architects, 2020).
25. Katzer, J. & Skoratko, A. Using 3d printed formworks for the creation of steel fibre reinforced concrete-plastic columns. *Constr. Build. Mater.* **337**, 127586 (2022).
26. Hack, N., Lauer, W., Gramazio, F. & Kohler, M. Mesh mould: robotically fabricated metal meshes as concrete formwork and reinforcement. In *Proceedings of the 11th International Symposium on Ferrocement and 3rd ICTRC International Conference on Textile Reinforced Concrete*, 347–359 (Rilem Publications Aachen, 2015).
27. Hack, N. & Lauer, W. V. Mesh-mould: robotically fabricated spatial meshes as reinforced concrete formwork. *Architectural Des.* **84**, 44–53 (2014).
28. Hack, N. et al. Mesh mould: an on site, robotically fabricated, functional formwork. In *Second Concrete Innovation Conference (2nd CIC)*, vol. 19, 1–10 (2017).
29. Gericke, O., Kovaleva, D., Haase, W. & Sobek, W. Fabrication of concrete parts using a frozen sand formwork. In *Proceedings of IASS Annual Symposia*, vol. 2016, 1–10 (International Association for Shell and Spatial Structures (IASS), 2016).
30. Li, W., Lin, X. & Xie, Y. M. A sustainable formwork system based on ice pattern and sand mould for fabricating customised concrete components. *Rapid Prototyp. J.* **29**, 639–654 (2023).
31. Liebringshausen, A., Eisenbach, P. & Grohmann, M. Re-usable concrete formwork system made of sand and wax. In *Proceedings of IASS Annual Symposia*, vol. 2017, 1–9 (International Association for Shell and Spatial Structures (IASS), 2017).
32. Sitnikov, V. Ice formwork for high-performance concrete: A model of lean production for prefabricated concrete industry. In *Structures*, vol. 18, 109–116 (Elsevier, 2019).
33. Sitnikov, V. & Rogers, P. Preliminary assessment of environmental performance of ice formwork production method for irregular architectural elements of concrete. *Int. J. Space Struct.* **36**, 78–87 (2021).
34. Sitnikov, V. Ice formwork for high-performance concrete: a model of lean production for prefabricated concrete industry. In *Proceedings of IASS Annual Symposia*, vol. 2018, 1–8 (International Association for Shell and Spatial Structures (IASS), 2018).
35. Kannan, M. R. & Santhi, M. H. Constructability assessment of climbing formwork systems using building information modeling. *Procedia Eng.* **64**, 1129–1138 (2013).
36. Li, S. et al. Study on construction technology of hydraulic climbing formwork for super high-rise building under aluminum formwork system. In *IOP Conference Series: Earth and Environmental Science*, vol. 769, 032062 (IOP Publishing, 2021).
37. Yao, G., Guo, H., Yang, Y., Xiang, C. & Robert, S. Dynamic characteristics and time-history analysis of hydraulic climbing formwork for seismic motions. *Adv. Civ. Eng.* **2021**, 2139153 (2021).
38. Panesar, D. & Shindman, B. The effect of segregation on transport and durability properties of self consolidating concrete. *Cem. Concr. Res.* **42**, 252–264 (2012).
39. Ley-Hernandez, A. M., Feys, D. & Hartell, J. A. Effect of dynamic segregation of self-consolidating concrete on homogeneity of long pre-cast beams. *Mater. Struct.* **52**, 1–22 (2019).
40. Breul, P., Geoffray, J.-M. & Haddani, Y. On-site concrete segregation estimation using image analysis. *J. Adv. Concr. Technol.* **6**, 171–180 (2008).
41. Ling, Y. & Leo, K. Reusing timber formwork: importance of workmen's efficiency and attitude. *Build. Environ.* **35**, 135–143 (2000).
42. Mei, Z., Xu, M., Luo, S., Tan, Y. & Li, H. Concrete formwork reuse in a supply chain with dynamic changes using ABMS and discrete events. *J. Clean. Prod.* **332**, 130038 (2022).
43. Pronk, A., Brancart, S. & Sanders, F. Reusing timber formwork in building construction: Testing, redesign, and socio-economic reflection. *Urban Plan.* **7**, 81–96 (2022).
44. Balasbaneh, A. T., Sher, W. & Ibrahim, M. H. W. Life cycle assessment and economic analysis of reusable formwork materials considering the circular economy. *Ain Shams Eng. J.* **15**, 102585 (2024).
45. Zhang, K. et al. Aerial additive manufacturing with multiple autonomous robots. *Nature* **609**, 709–717 (2022).
46. De Schutter, G. et al. Vision of 3d printing with concrete—technical, economic and environmental potentials. *Cem. Concr. Res.* **112**, 25–36 (2018).
47. Buswell, R. A., De Silva, W. L., Jones, S. Z. & Dirrenberger, J. 3d printing using concrete extrusion: a roadmap for research. *Cem. Concr. Res.* **112**, 37–49 (2018).
48. Xiao, J. et al. Large-scale 3d printing concrete technology: current status and future opportunities. *Cem. Concr. Compos.* **122**, 104115 (2021).
49. Wang, X. et al. Concrete 3d printing technology in sustainable construction: a review on raw materials, concrete types and performances. *Dev. Built Environ.* **9**, 100378 (2024).
50. Wang, L., Ma, G., Liu, T., Buswell, R. & Li, Z. Interlayer reinforcement of 3d printed concrete by the in-process deposition of U-nails. *Cem. Concr. Res.* **148**, 106535 (2021).
51. Baz, B., Aouad, G., Khalil, N. & Remond, S. Inter-layer reinforcement of 3d printed concrete elements. *Asian J. Civ. Eng.* **22**, 341–349 (2021).
52. Bos, F. P., Ahmed, Z. Y., Wolfs, R. J. & Salet, T. A. 3d printing concrete with reinforcement. In *High Tech Concrete: Where Technology and Engineering Meet: Proceedings of the 2017 fib Symposium, held in Maastricht, The Netherlands, June 12-14, 2017*, 2484–2493 (Springer, 2018).
53. Bos, F. P., Ahmed, Z. Y., Jutinov, E. R. & Salet, T. A. Experimental exploration of metal cable as reinforcement in 3d printed concrete. *Materials* **10**, 1314 (2017).
54. Kloft, H., Empelmann, M., Hack, N., Herrmann, E. & Lowke, D. Reinforcement strategies for 3d-concrete-printing. *Civ. Eng. Des.* **2**, 131–139 (2020).
55. Kromoser, B. & Kollegger, J. Pneumatic forming of hardened concrete–building shells in the 21st century. *Struct. Concr.* **16**, 161–171 (2015).
56. Kromoser, B. & Huber, P. Pneumatic formwork systems in structural engineering. *Adv. Mater. Sci. Eng.* **2016**, 4724036 (2016).
57. Kromoser, B., Pachner, T., Tang, C., Kollegger, J. & Pottmann, H. Form finding of shell bridges using the pneumatic forming of hardened concrete construction principle. *Adv. Civ. Eng.* **2018**, 6309460 (2018).
58. Kromoser, B. & Kollegger, J. Efficient construction of concrete shells by pneumatic forming of hardened concrete: Construction of a concrete shell bridge in Austria by inflation. *Struct. Concr.* **21**, 4–14 (2020).
59. Melancon, D., Gorissen, B., García-Mora, C. J., Hoberman, C. & Bertoldi, K. Multistable inflatable origami structures at the metre scale. *Nature* **592**, 545–550 (2021).

60. Veksler, Y., Ben-Abu, E. & Gat, A. D. Fluid-driven director-field design enables versatile deployment of multistable structures. *Adv. Intellig. Syst.* **6**, 2400179 (2024).
61. Ben Abu, E., Veksler, Y., Elbaz, S., Zigelman, A. & Gat, A. D. Growing structure based on viscous actuation of constrained multistable elements. *Adv. Mater. Technol.* **8**, 2202184 (2023).
62. Filipov, E. T., Tachi, T. & Paulino, G. H. Origami tubes assembled into stiff, yet reconfigurable structures and metamaterials. *Proc. Natl. Acad. Sci. USA* **112**, 12321–12326 (2015).
63. Zhu, Y. & Filipov, E. T. Large-scale modular and uniformly thick origami-inspired adaptable and load-carrying structures. *Nat. Commun.* **15**, 2353 (2024).
64. Li, Y. et al. Adaptive hierarchical origami-based metastructures. *Nat. Commun.* **15**, 6247 (2024).
65. Li, Z., Chen, W. & Hao, H. Dynamic crushing and energy absorption of foam filled multi-layer folded structures: experimental and numerical study. *Int. J. Impact Eng.* **133**, 103341 (2019).
66. Li, Z., Chen, W. & Hao, H. Functionally graded truncated square pyramid folded structures with foam filler under dynamic crushing. *Compos. Part B: Eng.* **177**, 107410 (2019).
67. Xiao, Y. et al. Optimization design of crashworthiness of polyurethane foam filled origami thin wall square tube based on a surrogate model. In *Structures*, vol. 65, 106713 (Elsevier, 2024).
68. Li, S., Fang, H., Sadeghi, S., Bhovad, P. & Wang, K.-W. Architected origami materials: how folding creates sophisticated mechanical properties. *Adv. Mater.* **31**, 1805282 (2019).
69. Chen, T., Bilal, O. R., Lang, R., Daraio, C. & Shea, K. Autonomous deployment of a solar panel using elastic origami and distributed shape-memory-polymer actuators. *Phys. Rev. Appl.* **11**, 064069 (2019).
70. Cai, J., Deng, X., Feng, J. & Zhou, Y. Geometric design and mechanical behavior of a deployable cylinder with Miura origami. *Smart Mater. Struct.* **24**, 125031 (2015).
71. Sharma, H. & Upadhyay, S. H. Folding pattern design and deformation behavior of origami based conical structures. *Adv. Space Res.* **67**, 2058–2076 (2021).
72. Wang, Q. et al. Geometric design and energy absorption of a new deployable cylinder tube. *Mech. Adv. Mater. Struct.* **29**, 1911–1924 (2022).
73. Tomita, S. et al. Origami-inspired metamaterials with switchable energy absorption based on bifurcated motions of a tachi-miura polyhedron. *Mater. Des.* **225**, 111497 (2023).
74. Peretz, O., Ben Abu, E., Zigelman, A., Givli, S. & Gat, A. D. A metafluid with multistable density and internal energy states. *Nat. Commun.* **13**, 1810 (2022).
75. Peretz, O., Abu, E. B., Zigelman, A., Givli, S. & Gat, A. D. Multistable metafluid based energy harvesting and storage. *Adv. Mater.* **35**, 2301483 (2023).
76. Ben-Abu, E. et al. Reprogrammable 3d shapes from 1d metamaterial. *Adv. Mater. Technol.* **10**, 2401113 (2025).
77. Breitman, P. et al. Flows in straws: viscous flows in one-dimensional metamaterial. *Phys. Rev. Appl.* **18**, 064077 (2022).
78. Younis, A. & Dodoo, A. Cross-laminated timber for building construction: a life-cycle-assessment overview. *J. Build. Eng.* **52**, 104482 (2022).
79. Alsabri, A. & Al-Ghamdi, S. G. Carbon footprint and embodied energy of pvc, pe, and pp piping: Perspective on environmental performance. *Energy Rep.* **6**, 364–370 (2020).
80. Guerra, F. B., Cavalcante, R. M. & Young, A. F. Green propylene and polypropylene production from glycerol: process simulation and economic evaluation. *ACS Sustain. Chem. Eng.* **11**, 2752–2763 (2023).

Acknowledgements

E.B.A. is grateful to the Azrieli Foundation for the award of an Azrieli Fellowship.

Author contributions

E.B.A., H.L., and A.D.G. conceived the research subject. E.B.A. constructed the experimental setup and conducted the experiments. A.Z. performed the theoretical analysis and numerical computations. E.B.A., A.Z., H.L., and A.D.G. wrote the paper.

Funding

This work was supported by the Azrieli Foundation through an Azrieli Fellowship awarded to E.B.A.

Competing interests

The authors declare the following competing interest: a U.S. provisional patent application (No. 63/928,607), entitled "Self-Deploying Formworks and Methods of Using the Same", has been filed by Columbia University and the Technion Research & Development Foundation based on technology related to this work. E.B.A., A.D.G., and H.L. are listed as inventors. All other authors declare no competing interests.

Consent for publication

Consent for publication was obtained from all identifiable individuals appearing in the figures.

Additional information

Supplementary information The online version contains supplementary material available at https://doi.org/10.1038/s44172-026-00725-1.

Correspondence and requests for materials should be addressed to Ezra Ben-Abu.

Peer review information *Communications Engineering* thanks Olga Beatrice Carcassi and the other, anonymous, reviewer(s) for their contribution to the peer review of this work. Primary Handling Editors: [Ali Behnood] and [Philip Coatsworth]. A peer review file is available.

Reprints and permissions information is available at http://www.nature.com/reprints

Publisher's note Springer Nature remains neutral with regard to jurisdictional claims in published maps and institutional affiliations.

Open Access This article is licensed under a Creative Commons Attribution-NonCommercial-NoDerivatives 4.0 International License, which permits any non-commercial use, sharing, distribution and reproduction in any medium or format, as long as you give appropriate credit to the original author(s) and the source, provide a link to the Creative Commons licence, and indicate if you modified the licensed material. You do not have permission under this licence to share adapted material derived from this article or parts of it. The images or other third party material in this article are included in the article's Creative Commons licence, unless indicated otherwise in a credit line to the material. If material is not included in the article's Creative Commons licence and your intended use is not permitted by statutory regulation or exceeds the permitted use, you will need to obtain permission directly from the copyright holder. To view a copy of this licence, visit http://creativecommons.org/licenses/by-nc-nd/4.0/.

© The Author(s) 2026